Global Change Biology Communications

WILEY

Global Change Biology Communications
BIOLOGY FOR A RAPIDLY CHANGING WORLD

RESEARCH ARTICLE OPEN ACCESS

Thermal Stress Is Associated With Fragmentation of Mediterranean *Posidonia oceanica* Meadows

Àlex Giménez-Romero[1,2] | Tomàs Sintes[2] | Carlos M. Duarte[3] | Manuel A. Matías[2]

[1]Department of Ecology and Complexity, Centro de Estudios Avanzados de Blanes (CEAB-CSIC), Blanes, Girona, Spain | [2]Instituto de Física Interdisciplinar y Sistemas Complejos (IFISC, CSIC-UIB), Palma de Mallorca, Spain | [3]Biological and Environmental Science and Engineering Division, King Abdullah University of Science and Technology (KAUST), Thuwal, Kingdom of Saudi Arabia

Correspondence: Àlex Giménez-Romero (alex.gimenez@csic.es)

Received: 6 March 2026 | **Revised:** 25 May 2026 | **Accepted:** 28 May 2026

ABSTRACT

Posidonia oceanica meadows, which underpin Mediterranean coastal ecosystems, are undergoing accelerated decline, partly driven by thermal stress. While previous quantitative studies have identified temperature thresholds beyond which seagrass mortality increases sharply, we assess the cumulative and sublethal impacts of prolonged warming under fluctuating subthreshold conditions. To capture these effects, we introduce Stress Degree Days (SDD), a physiologically grounded index derived from an experimentally derived mortality rate function. Using sea surface temperature (SST) data, we quantified the cumulative thermal exposure across the Mediterranean Basin from 2000 to 2020. Leveraging high-resolution satellite imagery and deep learning–based habitat mapping, we linked SDD-derived thermal exposure to meadow fragmentation, which is a proxy for seagrass health. Our results show that high thermal stress (> 50%) is concentrated along the southern and eastern Mediterranean, where meadows exhibit more than 40% cover loss and elevated fragmentation, even though maximum SSTs remained below lethal limits ($LT_{50} = 28.9°C$). This finding suggests that chronic sublethal thermal stress might play an important role in meadow structural degradation. Scenario-based projections under the RCP8.5, "business as usual", and the more moderate RCP4.5 climatic scenarios suggest basin-wide regression, with expected cover losses of approximately 80% and 40%, respectively, by 2100, and a strong contraction of suitable thermal conditions in southern regions. Consequently, fragmentation indices are projected to increase substantially, potentially affecting clonal connectivity, sediment retention, and oxygen export. In summary, by integrating physiological mechanisms, large-scale remote sensing, and climate modeling, the SDD framework identifies thermal hotspots, reveals emergent vulnerability patterns, and offers a risk-assessment tool to guide conservation strategies in warming oceans.

1 | Introduction

Seagrass meadows are foundational coastal ecosystems that sustain marine environments across all continents except Antarctica. These ecosystems provide essential services for human health, livelihoods, biodiversity, and climate regulation (Millennium Ecosystem Assessment 2005; Barbier et al. 2011; Duarte et al. 2025). The dense canopies of seagrass meadows support coastal biodiversity by providing food and habitat for numerous marine species, including commercially valuable ones. Moreover, seagrasses play a crucial role in sediment stabilization and coastal protection by reducing wave and current impacts (Granata et al. 2001; Koch et al. 2006), promoting sediment deposition (Gacia and Duarte 2001; Bos et al. 2007; Hendriks et al. 2008), and anchoring the seabed through extensive rhizome networks (Madsen et al. 2001). Furthermore, seagrasses are among the most effective natural carbon sinks on Earth, sequestering atmospheric CO_2 in both above- and belowground biomass and in long-lived sediment pools (Duarte and Chiscano 1999; Mcleod et al. 2011; Duarte, Sintes, and Marbà 2013). Despite their immense ecological and economic value, seagrass meadows are declining globally, with approximately one-third of the global area lost since

This is an open access article under the terms of the Creative Commons Attribution License, which permits use, distribution and reproduction in any medium, provided the original work is properly cited.

© 2026 The Author(s). *Global Change Biology Communications* published by John Wiley & Sons Ltd.

World War II (Duarte et al. 2025; Duarte, Losada, et al. 2013). The Mediterranean Basin has been particularly affected by local stressors impacting seagrass meadows, including eutrophication, habitat degradation, and mechanical disturbances, which are further compounded by climate change (Waycott et al. 2009).

The Mediterranean Sea is warming faster than the global ocean average, threatening endemic species such as *Posidonia oceanica*, the region's dominant seagrass species (Marbà and Duarte 2010; Jordà et al. 2012). Climate projections predict that rising sea surface temperatures (SST), particularly under the RCP8.5 scenario, will drastically reduce suitable habitats for *P. oceanica*, with niche models forecasting losses exceeding 75% by 2050 and potential functional extinction by 2100 (Chefaoui et al. 2018; Jorda et al. 2020). However, these estimates may be conservative, as they rely primarily on the maximum tolerable temperatures (thermal limits) for species survival, thereby neglecting cumulative sublethal thermal stress (Bennett et al. 2022). Seagrass thermal responses are typically inferred from laboratory experiments that expose plants to prolonged, constant temperatures to assess mortality and physiological performance (Savva et al. 2018). While these controlled experiments reveal fundamental thermal tolerance limits, they may not capture the cumulative stress imposed by the dynamic and fluctuating conditions that seagrasses encounter in the wild. In situ, seagrasses experience temporally variable temperature regimes, and mortality is likely the result of integrated stress over time rather than instantaneous threshold exceedance.

Recent advances in artificial intelligence (AI) and machine learning (ML) have enabled seagrass mapping using airborne and satellite imagery (Duarte et al. 2025), yielding promising but geographically constrained results (Chand and Bollard 2022; Jeon et al. 2021; Poursanidis et al. 2018; Traganos et al. 2018; Traganos and Reinartz 2018; Bakirman and Gumusay 2020; Kellaris et al. 2019; Chowdhury et al. 2024). Most existing models are designed for local applications and struggle to generalize across the diverse environmental conditions of the Mediterranean Basin, limiting their scalability for large-scale monitoring. Recently, however, a convolutional neural network model (CAMELE) has been developed to overcome this limitation (Giménez-Romero et al. 2025). CAMELE was trained on a geographically diverse benthic habitat dataset spanning the Balearic Islands, accounting for variations in water depth, water turbidity, and satellite viewing geometry, and was validated across independent regions. It achieved consistent segmentation performance for *Posidonia oceanica* cover at ecologically meaningful spatial scales, with an Intersection over Union (IoU) of 77.30% in regions substantially different from the training domain and up to 95.22% across the entire dataset. Because IoU jointly penalizes false positives and false negatives in the spatial overlap between predicted and reference masks, it is a more stringent metric for segmentation performance than overall classification accuracy (Rahman and Wang 2016). In semantic segmentation, IoU values above 50% are generally considered to indicate acceptable predictions (Dai et al. 2016). This open-source framework enables basin-wide assessments of seagrass distribution and structural changes, providing a baseline for evaluating climate-driven impacts, such as ocean warming and habitat fragmentation.

In this study, we integrated high-resolution remote-sensing-derived habitat maps from over 30 satellite images spanning diverse Mediterranean regions, generated using the CAMELE model, with historical sea surface temperature (SST) time series and experimental physiological data to resolve the impacts of cumulative thermal stress on *P. oceanica* meadows across the Mediterranean Sea. We introduce Stress Degree Days (SDD), a metric that quantifies thermal exposure by convolving daily SST data with an experimentally derived mortality rate curve, thereby capturing integrated thermal stress across natural variability. Using AI-driven habitat classifications, we computed seagrass cover and fragmentation across the Mediterranean Sea, revealing structural differences at basin-wide scales. Our results show that thermal stress is strongly associated with reduced cover and increased fragmentation, even though maximum SSTs remained below lethal limits, highlighting how sublethal thermal stress might affect ecosystem resilience. This integrated approach, which combines physiology, remote sensing, and modeling, provides a physiologically informed risk-assessment framework to understand seagrass decline in warming oceans, identifying emergent patterns beyond simplistic thresholds, and guiding targeted conservation initiatives amid escalating biodiversity threats.

2 | Results

2.1 | Quantifying Thermal Stress in the Mediterranean Sea

We developed a physiological model to estimate the cumulative thermal stress experienced by *Posidonia oceanica* meadows across the Mediterranean Sea. The model integrates daily sea surface temperature (SST) data with an experimentally derived mortality-rate function to compute a time-accumulated index of thermal exposure, which we term *Stress Degree Days* (SDD) (Figure 1a,b; Section 4). Using experimental data from 25-day exposures of *P. oceanica* shoots to constant temperature conditions, the accumulated SDD values were linked to observed shoot mortality through a logistic relationship (Figure 1c). When applied to spatially and temporally resolved SST data, the resulting quantity—hereafter referred to as thermal stress—is a model-based proxy for the expected shoot mortality associated with cumulative thermal exposure.

By integrating both the magnitude and duration of supra-optimal temperatures, this metric captures the progressive physiological burden imposed by warming under naturally fluctuating field conditions. In this sense, the SDD approach is similar to the degree heating weeks and days metric of stress, developed to predict the risk of bleaching and mortality in corals, which provides the basis for many models projecting future coral loss cover under climate change (Klein et al. 2024).

In contrast to traditional threshold-based approaches, which treat thermal stress as a discrete exceedance of fixed temperature limits, our framework explicitly accounts for the cumulative nature of thermal stress over time. The model shows that the maximum monthly average temperature (SST_{max}), a commonly used proxy for thermal stress, exhibits a logistic relationship with the SDDs (Figure 1d). However, our findings indicate that focusing exclusively on lethal temperature thresholds, such as the experimentally derived $LT_{50} = 28.9°C$,

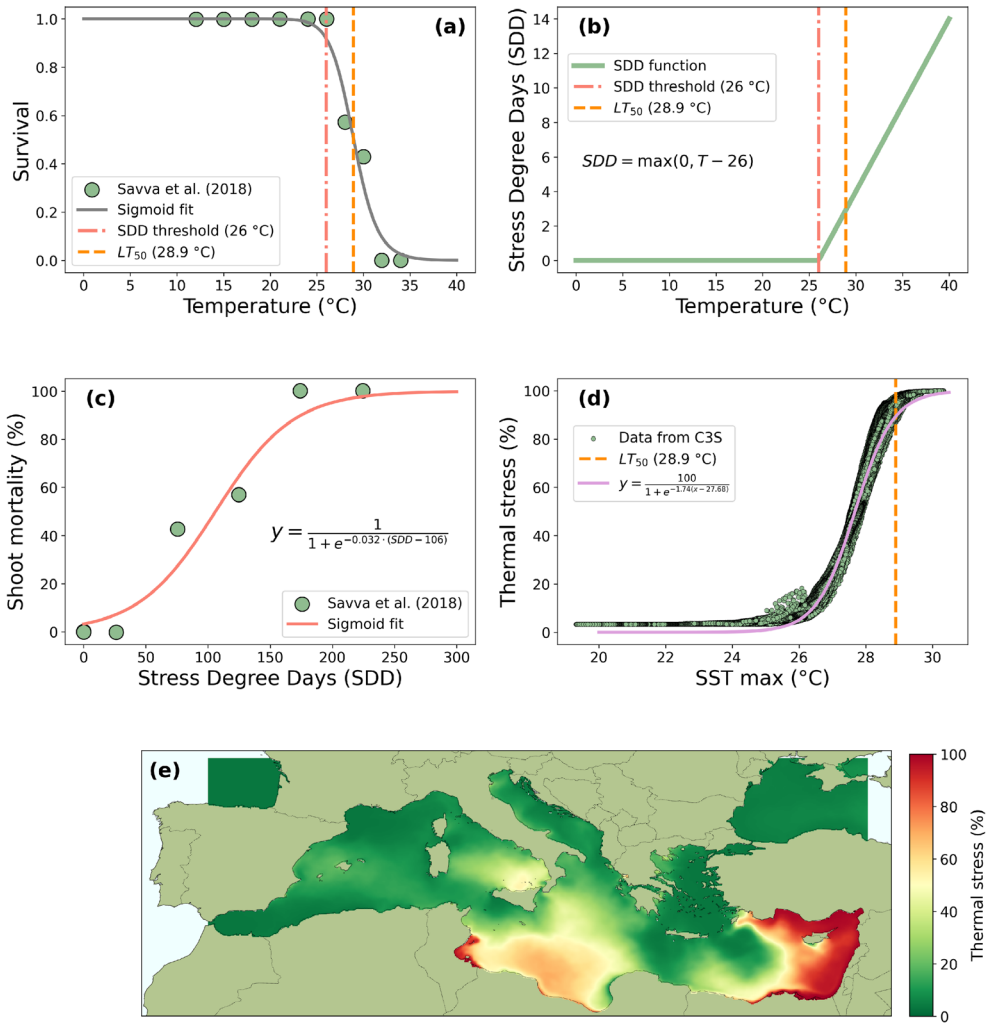

FIGURE 1 | Temperature-dependent mortality model for *Posidonia oceanica*. (a) Experimental survival of *Posidonia oceanica* shoots after 25 days of exposure to constant temperatures, based on data from (Savva et al. 2018). The dashed-dotted red line denotes the threshold below which mortality was not observed and is used to compute thermal stress. The orange dashed line, LT_{50}, corresponds to the lethal temperature threshold employed in previous studies to quantify the mortality risk in *Posidonia oceanica* based on the maximum SST (Savva et al. 2018). (b) Stress Degree Days (SDD) as a function of temperature with a threshold of $T = 26$°C recalculated from the experimental data, which showed negligible mortality below 26°C and a steep increase at higher temperatures. (c) Logistic fit of experimentally measured shoot mortality after 25 days under constant temperature conditions to SDD, computed from the experimental temperatures. (d) Thermal stress (expressed as predicted shoot mortality) as a function of the maximum SST across a 5 km grid in the Mediterranean Sea (green dots), showing a logistic relationship (pink line). We observe that the commonly used thermal limit LT_{50} captures only the highest percentile of thermal stress. (e) Spatial distribution of the average thermal stress in the Mediterranean Sea in the period 2000–2020.

provides an incomplete view of the stress dynamics. These thresholds capture only the uppermost tail of the thermal stress distribution (above the 90th percentile). In contrast, substantial cumulative stress can still accumulate in regions where SST_{max} remains below the lethal limits. This highlights the importance of accounting for sublethal and time-dependent effects when assessing the vulnerability of seagrass ecosystems to warming.

Using the dependence of thermal stress on SDDs, we generated spatially explicit maps of thermal stress across the entire Mediterranean Basin, utilizing daily SST data from the Copernicus Climate Change Service (C3S) for the period 2000–2020 (see Section 4). Our spatial analysis showed that areas of high cumulative thermal stress (i.e., > 50%) are currently concentrated along the southern and eastern coasts of the Mediterranean, particularly off Tunisia, Libya, Egypt, Gaza, Lebanon, Syria, and Turkey (Figure 1e). According to our analysis, these regions correspond to zones where sustained exposure to elevated temperatures has already exceeded the physiological tolerance limits inferred from experimental data, suggesting that these meadows may approach critical thresholds of decline under future climate conditions.

2.2 | The Impact of Thermal Stress in *Posidonia oceanica*

We integrated satellite-derived habitat classifications with the SDD metric generated by our physiological model to

examine the relationship between cumulative thermal stress and the spatial structure of *Posidonia oceanica* meadows across the Mediterranean Basin. To this end, for each study site, *P. oceanica* cover was estimated using our deep learning framework (Giménez-Romero et al. 2025), which provides spatially consistent estimates of the extent of seagrass from multispectral satellite imagery (see Figures S1–S3 for examples of habitat mapping). Meadow fragmentation was quantified using two complementary indices that capture distinct aspects of spatial configuration: (i) a gap-weighted fragmentation index (FI) sensitive to the size and shape of internal sand gaps within meadows and (ii) a composite fragmentation index derived from standardized landscape metrics describing patch density, subdivision, and compactness (see Section 4). Together, these metrics of fragmentation provide complementary quantification of meadow structure across spatial scales and environmental settings.

Our results revealed a clear correspondence between cumulative thermal stress and seagrass landscape configuration (Figure 2). The distribution of thermal stress across the Mediterranean Sea (Figure 1e) was broadly aligned with the landscape configuration of the seagrass meadows. Areas of elevated stress were concentrated along the southern and eastern coasts, particularly in the Levantine and Tunisian regions (Figure 2a), where sampled meadows tended to show lower seagrass cover and higher fragmentation (Figure 2b,c). These results suggest that meadows exposed to sustained sublethal warming exhibit marked structural degradation.

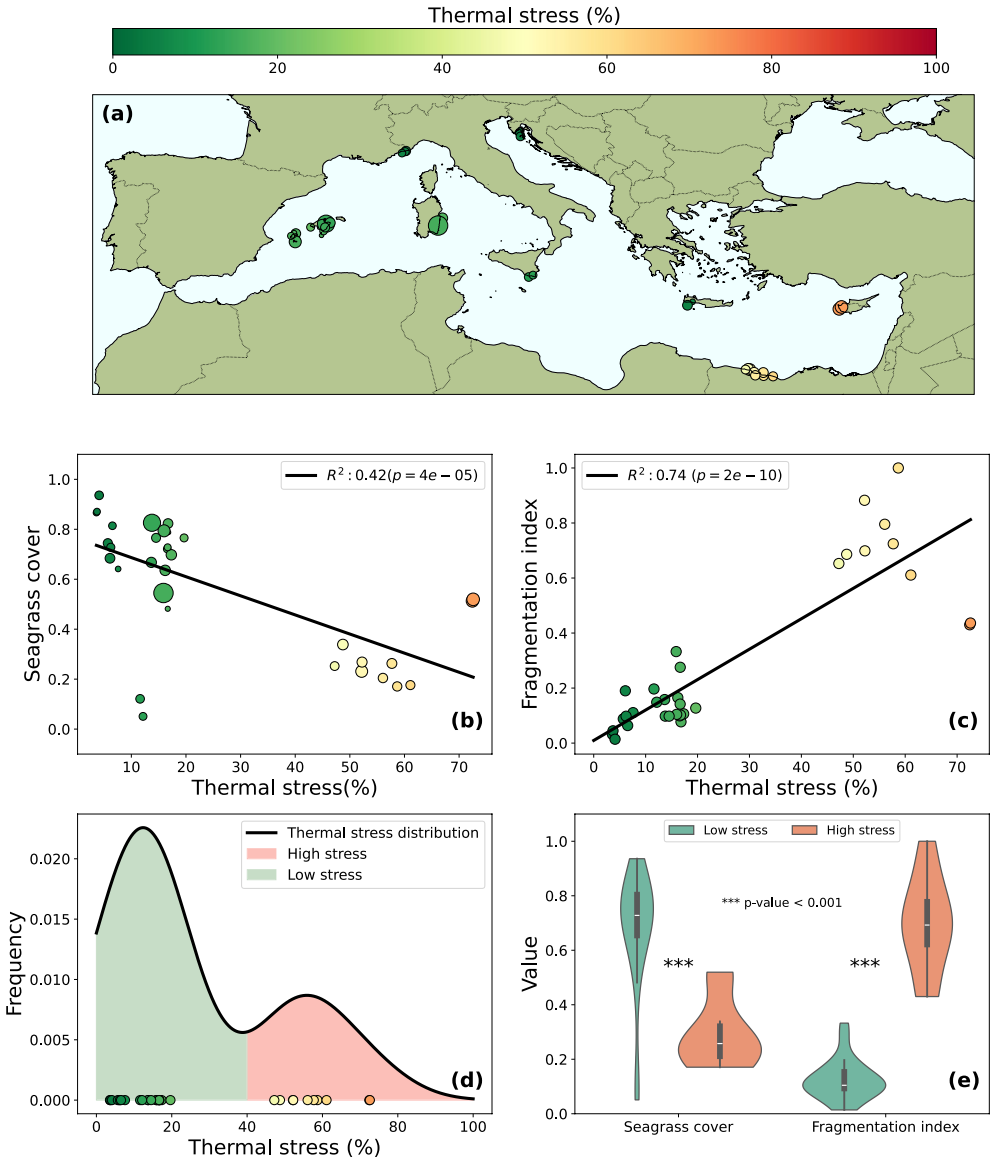

FIGURE 2 | Relationship between sea surface temperature, thermal stress, and *Posidonia oceanica* cover. (a) Locations where satellite imagery was obtained. The color indicates the estimated thermal stress for *Posidonia oceanica* meadows based on the historical SST data. (b) Scatter plot of seagrass cover versus thermal stress, showing a clear negative correlation. (c) Scatterplot of seagrass fragmentation versus thermal stress, showing a clear positive correlation. (d) The distribution of thermal stress across all sites highlights two stress groups identified from the empirical distribution of thermal stress values: Low (green) and high (red) stress (separated by a thermal stress level of 40%), which were used to categorize the sampling locations. (e) Violin plots of the distribution of seagrass cover and fragmentation in the two identified regions of thermal stress in our dataset. Regression statistics (R^2, p-values) are indicated where applicable.

Categorizing the sites further quantified the relationship between thermal stress and meadow conditions into low- and high-stress regimes based on the bimodal distribution of SDD values (Figure 2d). Both *P. oceanica* cover and the two fragmentation indices differed significantly between these regimes (Kruskal–Wallis test: $p < 0.001$; Figure 2e). On average, meadows located in high thermal stress regions displayed a reduction in cover exceeding 40% relative to low thermal stress areas, together with an increase of more than two-fold in fragmentation scores. The two meadow fragmentation metrics yielded consistent results, with both the gap-weighted FI and composite index showing a monotonic increase with cumulative thermal stress (Figure S10).

Notably, these spatial patterns emerged even in locations where the maximum monthly sea surface temperature (SST_{max}) remained below the experimentally determined lethal temperature threshold (LT_{50}) for *P. oceanica* (Figure S8). This suggests that substantial structural deterioration of meadows can occur under persistent sublethal thermal conditions, as captured by the cumulative stress metric. Overall, the basin-wide analysis revealed a clear spatial separation in meadow condition along a thermal stress gradient, supporting the utility of the SDD-based approach for identifying areas where cumulative warming is associated with reduced meadow integrity.

As an independent consistency check, we compared site-level SDD estimates with published field observations of *P. oceanica* decline across the Mediterranean (Marbà et al. 2013, 2014). Although these datasets differ in sampling design, response variable, temporal window, and local disturbance context, they provide an external test of whether higher cumulative thermal exposure is associated with observed meadow deterioration (Supporting Information Section 3). Across the available field metrics, the relationships were generally in the expected direction: higher SDD and thermal stress values were associated with reduced shoot density and increased meadow loss or degradation (Figures S5–S7). Despite the limitations of this comparison, shoot density change showed weak but statistically significant negative correlations with both SDD and SDD-derived thermal stress ($R = -0.32$ and $R = -0.24$, respectively; $p < 0.05$ and $n = 58$), whereas several other field metrics exhibited larger absolute correlations but were not statistically significant.

2.3 | Projecting Seagrass Regression Under Climate Change

We then used the empirical relationship between meadow landscape configuration indices and thermal stress to estimate the trajectory of *Posidonia oceanica* meadows under projected Mediterranean warming conditions. We computed future thermal stress from projected SST data under two Representative Concentration Pathways (RCPs): RCP4.5, representing an intermediate emissions scenario, and RCP8.5, a high-emissions pathway assuming continued reliance on fossil fuels by the end of the century ("business-as-usual" scenario). These projections, derived from the Copernicus Marine Biogeochemistry dataset (Copernicus Climate Change Service 2020) (Section 4), enabled us to estimate cumulative thermal stress and the associated impacts on seagrass cover and fragmentation from 2006 to 2100.

Spatially resolved projections for 2100 revealed a pronounced projected escalation in thermal stress across the Mediterranean Basin, with the most severe impacts concentrated in the southern and eastern regions (Figure 3a). Under RCP4.5, thermal stress values are expected to exceed 80% along the coasts of Tunisia, Libya, Egypt, and the Levantine Sea, encompassing areas that currently support extensive *P. oceanica* meadows. This intensification of thermal stress translates to substantial habitat degradation, with potential reductions in seagrass cover exceeding 60% in these high-stress zones relative to present-day estimates (Figure 3b). Beyond the expected hotspots of thermal stress in the southern and eastern Mediterranean (Chefaoui et al. 2018; Litsi-Mizan et al. 2023), our projections revealed the development of intense, geographically constrained thermal hotspots and highlighted the critical importance of thermal refugia across the basin (Figure 3a). Even under the less severe RCP4.5 scenario, areas with previously low stress are projected to experience a sharp increase in cumulative thermal stress, potentially leading to meadow degradation. Notably, projections for 2100 show the emergence of new high-stress centers in the northern Mediterranean, particularly around the Balearic Islands and the southwestern coasts of Italy, where the cumulative thermal stress is expected to exceed the 50% threshold by a considerable margin. This northward and eastward expansion of thermal stress is therefore expected to contribute to the future spatial pattern of meadow degradation. Conversely, certain areas maintained remarkably low SDD values, even under the high-emissions RCP8.5 pathway (Figures S14 and S15). These include the coasts of southern Spain (Alboran Sea), southern France (Gulf of Lion), and parts of the Aegean Sea, suggesting that these regions could function as critical thermal refugia for *P. oceanica*, potentially safeguarding its presence in the Mediterranean. These areas are projected to warm less than other areas because of their distinct oceanographic regimes. The Alboran Sea is a frontal zone where the surface Atlantic and Mediterranean waters converge and often experience intense mixing due to several processes (Sánchez-Garrido and Nadal 2022), similar to the Gulf of Lion, which is affected by strong mistral winds leading to convective mixing (Schott et al. 1996), while the Aegean thermal refugia arise due to the interface cooling due to mixing by cyclones (Romanski et al. 2014). However, the persistence of these potential refugia will depend on future changes in circulation, stratification and vertical mixing, which may alter local thermal buffering.

The empirical link between high cumulative stress and meadow structural deterioration suggests that extensive areas projected to experience high SDD values could shift from relatively continuous meadows towards more fragmented landscapes (Figure S16). Previous work indicates that such configurations may be associated with reduced connectivity, altered meadow functioning, and lower resilience (Ruiz-Reynés et al. 2017; van de Vijsel et al. 2023), and this transition could be particularly acute in current and emerging thermal hotspots. By 2100, under the high-emissions scenario, the projected increase in structural fragmentation would imply a widespread shift towards lower-cover, higher-fragmentation seascapes across much of the

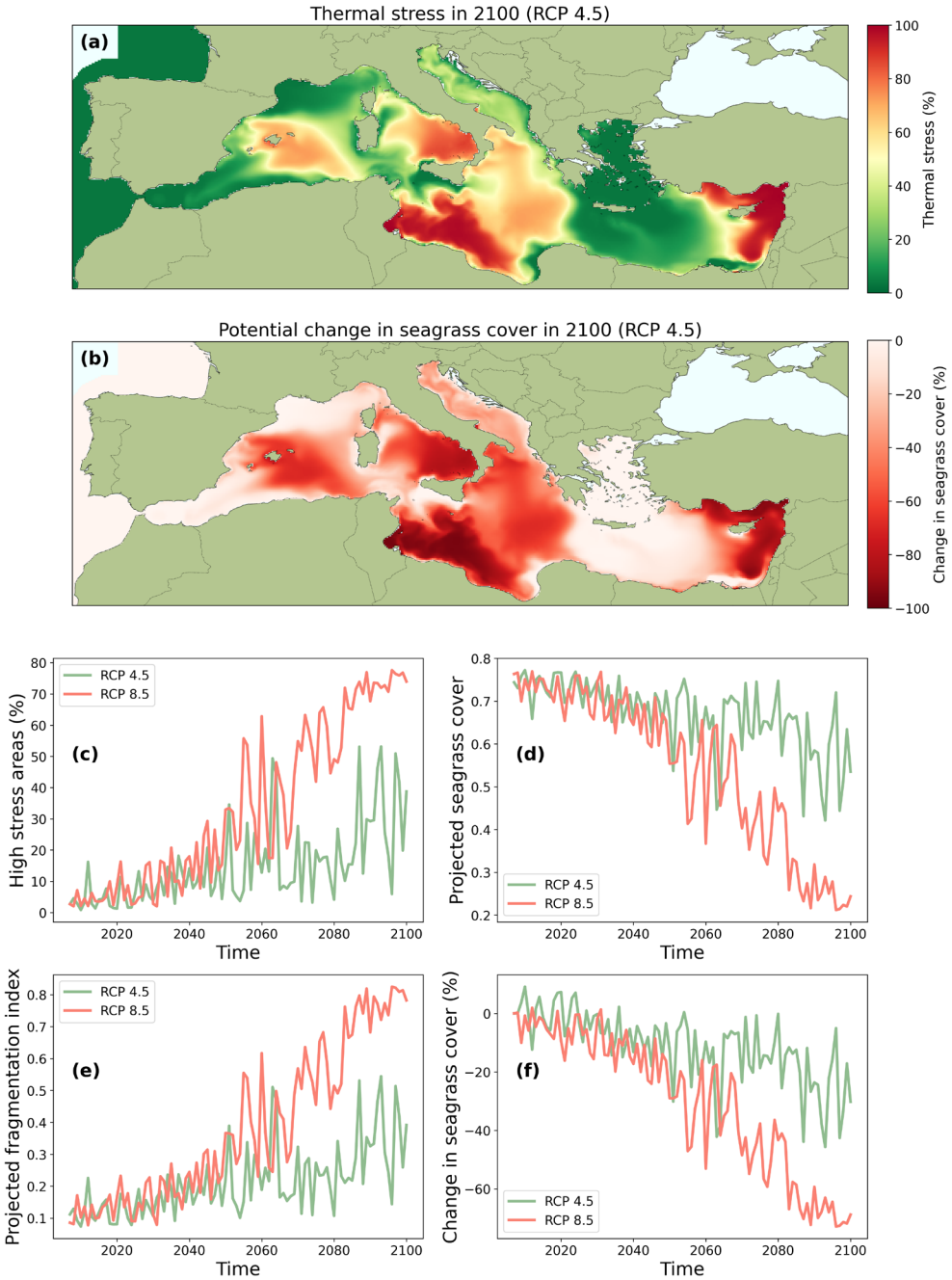

FIGURE 3 | Projected thermal stress and changes in *Posidonia oceanica* meadows under future climate scenarios. (a) Spatial distribution of cumulative thermal stress (SDD) across the Mediterranean Sea in 2100 under RCP4.5. (b) Potential change in seagrass cover (%) in 2100 under RCP4.5, relative to the 2020 baseline estimates. (c) Temporal evolution of the fraction of high-stress areas (> 50%) from 2020 to 2100 under RCP4.5 (green) and RCP8.5 (red). (d) Projected basin-wide seagrass cover from 2020 to 2100 under RCP4.5 (green) and RCP8.5 (red) emission scenarios. (e) Projected fragmentation index from 2020 to 2100 under RCP4.5 (green) and RCP8.5 (red). (f) Cumulative change in seagrass cover (%) from 2020 to 2100 under RCP4.5 (green) and RCP8.5 (red). Projections are based on SST data from the Copernicus Marine Biogeochemistry dataset (Copernicus Climate Change Service 2020), integrated with the SDD framework.

Mediterranean basin, with the greatest potential for persistent continuous cover concentrated in northern regions identified as relative thermal refugia (Figures S14–S16).

However, the specific fragmentation thresholds at which these structural changes translate into functional decline or collapse in Mediterranean *P. oceanica* meadows remain to be quantified. Therefore, these projections should be interpreted as indicators of increasing structural risk rather than as predictions of ecosystem functional collapse.

Projected temporal dynamics underscore progressive deterioration, with the fraction of high-stress areas (> 50%) expanding nonlinearly over the next few decades (Figure 3c). Under RCP4.5, this fraction is projected to increase from approximately 10% in 2020 to over 40% by 2100, whereas RCP8.5 accelerates

this trend, potentially affecting more than 50% of the basin by mid-century and approaching near-ubiquitous stress (> 70%) by 2100. Concomitantly, basin-wide seagrass cover is expected to decline steadily, with RCP4.5 yielding a 30%–40% reduction and RCP8.5 leading to estimated losses exceeding 70% by the end of the century (Figure 3d,f). Fragmentation indices mirror this regression, exhibiting a twofold to threefold increase under RCP4.5 and even steeper amplification under RCP8.5, consistent with an increasing tendency towards meadow disassembly into isolated patches (Figure 3e).

The preceding analysis focused on basin-scale average impacts; however, it is critical to recognize that thermal stress is inherently depth-dependent. As *P. oceanica* meadows can extend down to 50 m, we investigated how the projected cumulative thermal stress varies with depth under both RCP4.5 and RCP8.5 scenarios (Figures 4 and S17). Our results indicate that the shallowest depths (e.g., < 10 m) are projected to experience greater thermal stress than deeper zones (e.g., > 20 m) by 2100 (Figure 4a,b). While thermal stress values at 10 m frequently exceeded 70% across large areas, they were markedly attenuated at 20 m. This differential warming is quantified by the percentage of the Mediterranean seabed area falling into the high-stress category (> 50%) as a function of depth (Figure 4c). This analysis revealed a profound increase over time in the extent of high-stress zones, but with a sharp decline in vulnerability beyond approximately 20 m depth. For the period 2090–2100, the extent of the high-stress area is nearly four times greater at 10 m than at 30 m. A similar pattern is observed under the RCP8.5 scenario, albeit with a more pronounced increase in high-stress areas at shallower depths (Figure S17).

3 | Discussion

Our findings show that cumulative thermal stress, quantified using the Stress Degree Days (SDD) metric, provides a physiologically informed indicator of *Posidonia oceanica* meadow

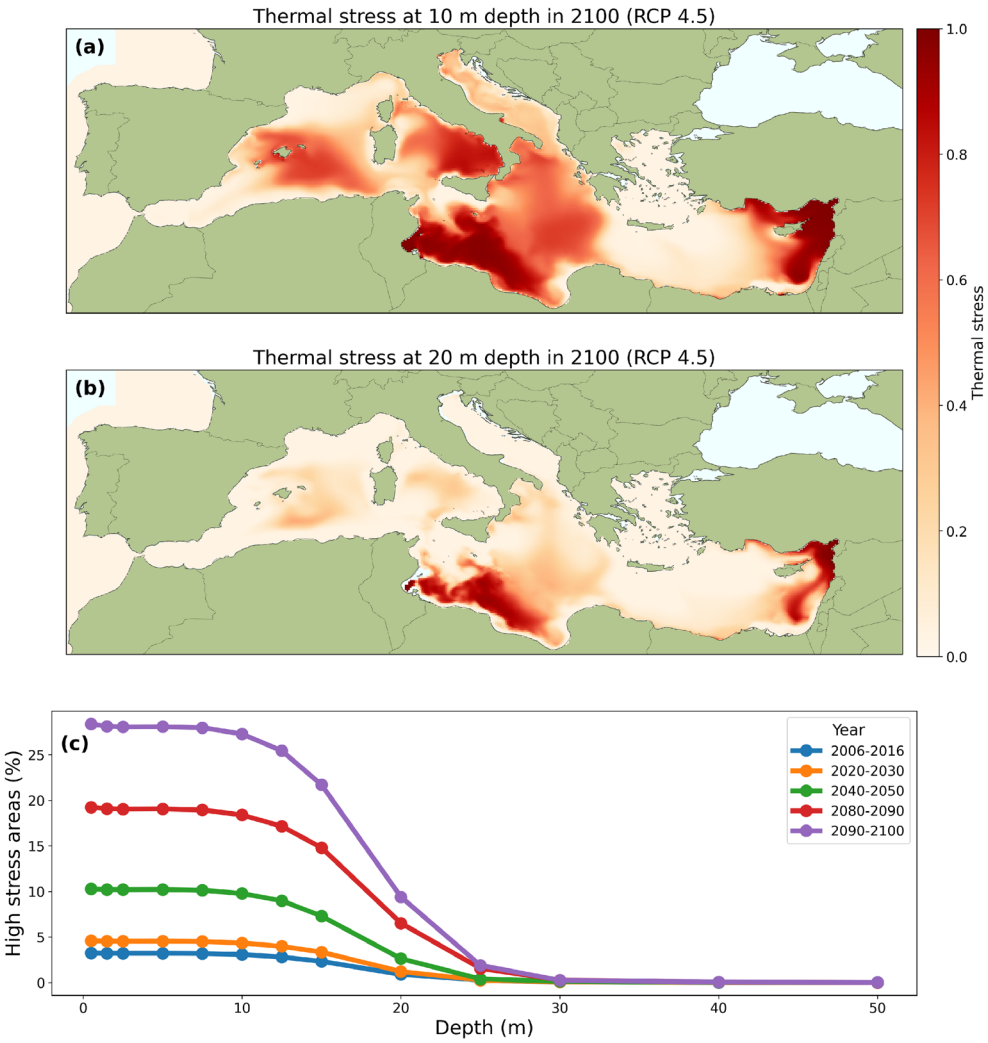

FIGURE 4 | Projected thermal stress across depths under the RCP4.5 scenario. (a) Spatial distribution of cumulative thermal stress (SDD) at 10 m depth in 2100 under the RCP4.5 scenario. The redder areas indicate higher thermal stress, ranging from 0 (no stress) to 1 (maximum stress). (b) Spatial distribution of cumulative thermal stress (SDD) at 20 m depth in 2100 under the RCP4.5 scenario, showing a reduced intensity compared to 10 m. (c) Average percentage of high-stress areas (> 50%) across the Mediterranean Sea as a function of depth for different time periods (2006–2016, 2020–2030, 2040–2050, 2080–2090, and 2090–2100). The plot illustrates a projected increase in high-stress areas over time, with a sharp decline in their extent beyond 20–30 m depth, highlighting the shallow-water vulnerability.

degradation across the Mediterranean Sea. By integrating experimental mortality data with temporally varying sea surface temperatures, the SDD approach effectively captures sublethal thermal stress, which is overlooked by traditional absolute-threshold-based metrics. This distinction is critical in naturally fluctuating marine environments, where prolonged exposure to moderately elevated temperatures induces progressive physiological damage, manifested as reduced shoot density, impaired growth, and potential meadow fragmentation. Recent empirical evidence supports this hypothesis. Marine heatwaves (MHWs) exacerbated by climate change impose cumulative sublethal stress on *P. oceanica*, triggering stress-induced adaptive responses such as profuse flowering, a stress-induced reproductive strategy (Marín-Guirao et al. 2019; Chimienti et al. 2025). Moreover, ontogeny-specific vulnerabilities reveal that seeds exhibit heightened sensitivity to thermal events (Rinaldi et al. 2023), reinforcing the importance of cumulative metrics, such as SDD, that integrate impacts across developmental stages. Consequently, our approach extends beyond previous threshold and thermal niche models, which likely underestimate the contribution of sublethal thermal stress to species decline (Catucci and Scardi 2020; Marbà et al. 2022).

The spatial patterns revealed in our analysis correspond closely with the documented declines in *P. oceanica* meadows in the southern and eastern Mediterranean (Litsi-Mizan et al. 2023), where warming rates are increasing most rapidly. Regions such as Tunisia, Libya, and the Levantine coast exhibit high SDD values and a prevalence of fragmented meadows with over 40% loss of cover, even where maximum temperatures remain below lethal limits. This indicates that chronic cumulative stress progressively undermines meadow resilience through processes such as inhibited clonal expansion and heightened vulnerability to feedback mechanisms (Ruiz-Reynés et al. 2017, 2023). Transcriptomic analyzes of simulated MHWs further revealed differential gene expression across stress intensities (Stipcich et al. 2024), reinforcing the notion that prolonged sublethal thermal stress can induce a physiological response, potentially leading to structural degradation. The ecological consequences of fragmentation extend beyond structural decline and affect ecosystem metabolism and resilience. Recent field evidence from Mediterranean *P. oceanica* meadows shows that moderate fragmentation (FI >3.4), combined with enhanced hydrodynamic flow, significantly increases dissolved oxygen concentrations through improved lateral advection and reduced boundary layer thickness, thereby enhancing both gross primary production and net community oxygenation (Mayol et al. 2026). This suggests a counterintuitive adaptive mechanism: while initial fragmentation accelerates clonal disconnection, it also boosts local productivity and oxygen export, which may support neighboring benthic communities and delay hypoxia-driven feedback in warming coastal embayments. However, this metabolic advantage is likely transient; as thermal stress intensifies and fragmentation exceeds critical thresholds, declining canopy complexity and rhizome connectivity ultimately impair carbon sequestration, sediment stabilization, and long-term resilience.

Projections under the RCP4.5 and RCP8.5 scenarios estimate severe habitat regression, with potential cover loss exceeding 70% under high-emission conditions. Such declines would likely increase meadow fragmentation and may increase the risk of severe regional functional loss, particularly in the southern basins (Jordà et al. 2012; Chefaoui et al. 2018). These projections align with broader trends across Mediterranean ecosystems, where synergistic stressors, including sea-level rise, invasive species, and marine heatwaves, can contribute to cascading biodiversity losses and reduce carbon sequestration (Marbà et al. 2015). Sustained warming may progressively simplify meadow architecture, with potential consequences for clonal connectivity and rhizome-mediated resource sharing. This breakdown can accelerate local extinction dynamics while eroding the genetic diversity essential for long-term adaptation (Kendrick et al. 2017). As canopy density declines, sediment retention capacity weakens, increasing erosion and turbidity and potentially inhibiting recolonization, thereby reinforcing feedback loops that strengthen habitat degradation. In semi-enclosed coastal systems, these structural losses could reduce the role of meadows as metabolic hotspots, diminishing oxygen export to adjacent habitats and weakening support for associated fauna. The convergence of thermal stress with co-occurring pressures ultimately risks pushing *P. oceanica* meadows beyond critical tipping points, fragmenting once-continuous seascapes into lower-functioning patches with diminished ecological roles (Ruiz-Reynés et al. 2023).

Although our model represents a significant advancement in quantifying cumulative thermal stress on *Posidonia oceanica* meadows by integrating experimental mortality data with satellite-derived sea surface temperature (SST) records, several limitations must be acknowledged to contextualize its applicability and guide future refinements. First, reliance on SST as a thermal proxy assumes uniform heat transfer to benthic habitats; however, this approach overlooks vertical thermal stratification. Deeper meadows, which often extend to 40 m or beyond (Telesca et al. 2015), may experience substantially cooler and more stable conditions than surface waters, potentially leading our model to underestimate the resilience of bathymetrically diverse sites. Our depth-resolved model reveals depth-dependent vulnerability, with shallow (<10 m) meadows likely to experience greater thermal stress and landscape fragmentation than deeper ones. Hence, our results suggest that shallow *P. oceanica* meadows are critically threatened by climate change and are likely to be the first to undergo severe structural fragmentation. Deeper meadows may provide refuge within particular regions, offering a narrow but increasingly important window of persistence for the species. However, shallow, <10 m, *P. oceanica* meadows play a disproportional role in coastal protection (Ondiviela et al. 2014). Accordingly, even where *P. oceanica* persists, reductions in shallow meadow cover could substantially weaken its coastal protection benefits.

The model was based on experimental data from the western Mediterranean (Balearic Islands) and may not necessarily apply to the entire range of *P. oceanica*. Unfortunately, the lack of controlled thermal experiments testing mortality responses to increasing temperatures precludes the testing of these models elsewhere. The existence of a thermal gradient reflected in increasing maximum temperatures from the western towards the eastern Mediterranean basin could imply the a priori expectations of eastern Mediterranean *P. oceanica* meadows are more resistant to thermal stress than those in the western Mediterranean. However, existing evidence does not suggest

the existence of such variability. For instance, reconstruction of growth dynamics in Greek *P. oceanica* populations concluded that maximum temperatures above 26.5°C caused a sharp decrease in production (Litsi-Mizan et al. 2023), indicating a threshold for sublethal thermal stress similar to that empirically resolved for western Mediterranean populations (Savva et al. 2018). Likewise, reciprocal transplant experiments across the western, central, and eastern Mediterranean (Bennett et al. 2024) and across cool subthermocline environments to warmer, shallower environments (Stipcich et al. 2023) did not show any correspondence between the thermal origin of the transplants and their performance. Hence, existing evidence does not reject the assumption of a consistent thermal response of *P. oceanica* across its entire distribution range.

Another limitation of our framework is that it does not explicitly account for the multi-stressor interactions prevalent in coastal ecosystems. Synergistic effects between warming and eutrophication can amplify nutrient toxicity and reduce plant performance under chronic co-exposure (Ontoria et al. 2019; Helber et al. 2021), while nocturnal hypoxia could lead to sulfide poisoning in seagrasses (Borum et al. 2005; Harald 2023). Similarly, herbivory may intensify under elevated temperatures, potentially exacerbating fragmentation through selective grazing (Santana-Garcon et al. 2023), while ocean acidification coupled with marine heatwaves (MHWs) impairs photosynthetic efficiency and seedling survival (Ravaglioli et al. 2024; Pazzaglia et al. 2025). These interactions could substantially modulate SDD estimates but remain unmodeled in the current framework, as they require local level knowledge of current and future stressors, which is lacking. However, increased awareness of the importance of *P. oceanica* is driving conservation efforts, particularly on the northern coast of the Mediterranean Basin (Rigo et al. 2021). Enhanced conservation management should reduce the local pressures exerted on these ecosystems, further supporting increased restoration efforts (Pansini et al. 2022).

The precision of the model reported here is further limited by constraints imposed by remote sensing. Our deep-learning-based habitat mapping is constrained by satellite imagery limitations, including atmospheric interference, water turbidity, depth-dependent light attenuation, and spectral confusion among benthic classes. Although CAMELE showed strong segmentation performance in independent validation and was robust across heterogeneous conditions (Giménez-Romero et al. 2025), these factors can substantially reduce segmentation performance. Turbidity, in particular, can obscure benthic features and increase the uncertainty in habitat classifications, especially in deeper or more dynamic coastal environments. This uncertainty in the predicted habitats can propagate to derived estimates of cover and fragmentation. This limitation is particularly relevant at meadow boundaries, around small internal gaps, and in spectrally ambiguous transition zones between *P. oceanica*, sand, macroalgae, and other benthic vegetation. Moreover, the 3–4 m resolution of PlanetScope data may fail to resolve fine-scale fragmentation patterns such as small canopy gaps or patchy die-offs, while fragmentation metrics are sensitive to the spatial scale at which they are calculated. Temporal mismatches between historical SST records (2000–2020) and recent imagery (2023) introduce additional uncertainty when linking current meadow states to past thermal stress, potentially overlooking recovery dynamics and lagged mortality responses. Finally, future projections under RCP4.5 and RCP8.5 inherit uncertainties from climate models (Power et al. 2017). The assumptions of static species distributions ignore potential range shifts, selection, and adaptive evolution (Jahnke et al. 2019), which may shift thermal sensitivity curves under future climate change, as reported for corals (Klein et al. 2024). This could lead to an overestimation of the decline in resilient populations or an underestimation of compounding factors, such as invasive species, that accelerate degradation.

More generally, a key limitation of our study is its focus on locations selected as relatively pristine, which was intended to reduce the confounding influence of direct human disturbance. Some sites may not be as undisturbed as presumed, and low-intensity or cryptic anthropogenic pressures—such as occasional anchoring, historical degradation, or diffuse coastal impacts—may still contribute to fragmentation patterns in ways not captured by our screening criteria. Consequently, while our results support an association between cumulative thermal stress and spatial degradation, the influence of undetected local disturbances cannot be ruled out entirely. Because the basin-wide relationships between SDD and meadow structure remain observational, definitive causal attribution of meadow fragmentation to thermal stress will require temporal replication, independent long-term monitoring, and ideally experimental or quasi-experimental tests that disentangle warming from local anthropogenic disturbances. In addition, while our study covers the entire Mediterranean basin, the validation was biased to the Western Mediterranean, where most of the data were present. Hence, we call for efforts to further validate the model, especially for the Eastern Mediterranean basin, which will require new data sets and collaborative efforts. Finally, our focus on minimally impacted sites implies that our estimates represent a conservative lower bound for the basin-wide drivers of degradation. In more heavily affected areas, where thermal stress interacts synergistically with local anthropogenic pressures, fragmentation rates may be higher, and ecological thresholds are likely to be reached more rapidly.

Addressing these limitations through integrated approaches, including in situ validation, multi-depth thermal profiling, coupled multi-stressor experiments, and the deployment of higher-resolution sensors, will substantially enhance the predictive accuracy. Likewise, future applications of this framework should explicitly integrate quantified gradients of human impact to disentangle better the interacting roles of warming and local stressors in seagrass fragmentation. Overall, we expect our modeling framework to inform adaptive management strategies for conserving this keystone species under accelerating climate change.

4 | Methods

4.1 | Temperature Data

We used sea surface temperature (SST) data from two complementary sources to quantify thermal exposure in the *Posidonia oceanica* meadows. For the historical analysis, we employed the

dataset "Sea surface temperature daily data from 1981 to present derived from satellite observations" (Copernicus Climate Change Service (C3S) 2019) provided by Copernicus Climate Change Service (C3S). This product provides daily global SST estimates derived from multiple infrared satellite sensors and processed using optimal interpolation techniques. The dataset merges multi-sensor inputs to produce spatially complete gap-free temperature fields on a regular 0.05° grid (~5 km resolution), ensuring consistent and homogeneous coverage across space and time.

For future climate projections, we used temperature data from the Copernicus dataset "Marine biogeochemistry data for the Northwest European Shelf and Mediterranean Sea from 2006 to 2100 derived from climate projections" (Copernicus Climate Change Service 2020). This dataset is based on simulations produced using the European Regional Seas Ecosystem Model (ERSEM v15.06) coupled with the regional ocean circulation models POLCOMS and NEMO through the FABM framework. The models account for physical processes (e.g., temperature, salinity, and currents) and biogeochemical cycles (e.g., nutrients and oxygen) and are forced by downscaled CMIP5 climate projections using the RCA4 atmospheric model. SST was extracted under two Representative Concentration Pathways (RCPs): RCP4.5 and RCP8.5. These projections were used to estimate future thermal stress values and assess potential impacts on seagrass fragmentation under climate change scenarios. The dataset provides daily temperature data on a regular 0.1° latitude–longitude grid (~10 km resolution) over the Mediterranean Basin for the period 2006–2100 at different depths.

For the surface-based historical analysis and for the main basin-scale projections of cover and fragmentation, we used the first available depth level ($z = 0.5$ m), to maintain consistency with the satellite-derived SST product used for the historical period. In addition, because the climate-projection dataset provides temperature fields across multiple depth levels, we repeated the future thermal-stress calculations across all available depths to assess the depth dependence of projected exposure. These depth-resolved analyzes were performed for both RCP4.5 and RCP8.5 and are presented in Figures 4 and S17.

4.2 | Modelling Seagrass Thermal Stress

To model the impact of thermal stress on *P. oceanica* cover, we used the experimental results from Savva et al. (2018), which quantified shoot mortality as a function of prolonged exposure to a constant temperature. Specifically, the authors reported the percentage of shoot mortality after 25 days of exposure to a constant temperature at multiple thermal levels. Thus, the results of the experiment represent the cumulative effect of a temperature-dependent mortality rate $\mu(T)$, which is constant over time in the experimental setup. However, seagrasses are exposed to time-varying temperatures throughout their lifetime; therefore, a model that accounts for the dynamic nature of thermal stress is necessary.

We modeled the thermal stress as the cumulative effect of a temperature-dependent mortality rate $\mu(T(t))$. We consider that, under stress, the shoot density of a seagrass population follows the dynamics

$$\frac{\mathrm{d}P}{\mathrm{d}t} = -\mu(T(t))P, \tag{1}$$

so that the shoot density at time t is obtained by solving the differential equation

$$P = P_0 \exp\left(-\int_0^t \mu(T(t))\mathrm{d}t\right) = P_0 \exp(-SDD). \tag{2}$$

Thus, Equation (2) models the potential exponential decrease in *Posidonia oceanica* shoot density as a function of cumulative temperature-dependent mortality $SDD = \int_0^t \mu(T(t))\mathrm{d}t$, hereafter called *Stress Degree Days*.

The temperature-dependent mortality rate $\mu(T)$ was extrapolated from the experimental results of Savva et al. (2018) by considering no stress below a certain threshold and a linearly increasing mortality rate with temperature above the threshold. Altogether, this is modeled using a nonlinear piecewise function,

$$\mu(T) = \begin{cases} 0 & \text{if} \quad T <= T^* \\ T - T^* & \text{if} \quad T > T^* \end{cases} = \max(0, T - T^*) \tag{3}$$

The value of the threshold, T^*, corresponds to the lowest temperature at which there is no mortality in the experiments of Savva et al. (2018), that is, $T = 26$°C (Figure 1a,b).

Finally, the accumulation of SDD was linked to the thermal stress by fitting a logistic curve to the experimental results of Savva et al. (2018) (Figure 1c). Because all experiments were performed for the same amount of time, $\Delta t = 25$ days, and at different constant temperatures, the SDD of each experiment is easily computed as,

$$SDD = \int_0^t \mu(T(t))dt = 25 \cdot \mu\left(T_{\text{experiment}}\right) = 25 \cdot \max\left(0, T_{\text{experiment}} - 26\right). \tag{4}$$

Finally, the relationship between SDD and experimentally-derived mortality is described by a logistic function, which allows the translation of the accumulated stress into an estimate of potential mortality (Figure S4), thereby named "thermal stress",

$$\text{thermal stress} = \frac{1}{1 + e^{-0.032(SDD-106)}}. \tag{5}$$

Details of the comparison between site-level SDD estimates and independent field observations of *P. oceanica* decline are provided in Supporting Information Section 3.

4.3 | Thermal Stress From SST Data

In practice, the integral of the time-varying mortality rate is obtained computationally from temperature data by approximating the integral by a summation,

$$SDD = \int_0^t \mu(T(t)) \approx \sum_{i=1}^{N} \mu(T_i) = \sum_{i=1}^{N} \max(0, T_i - 26), \tag{6}$$

where T_i corresponds to the daily SST values.

4.4 | Bathymetry Data

Bathymetry data were obtained from the European Marine Observation and Data Network (EMODNET) (Martín Míguez et al. 2019). EMODnet Bathymetry provides a service for viewing and downloading a harmonized Digital Terrain Model (DTM) for European sea regions. The data consisted of GeoTIFF layers with ~100 m pixel resolution of mean depth values, which were interpolated to the satellite imagery resolution.

4.5 | Satellite Data

Satellite imagery was obtained from Planet under the Education and Research Program, which provides limited, noncommercial access to PlanetScope and RapidEye imagery (Planet Team 2017). In particular, we acquired PlanetScope images from the Super Dove (PSB.SD) instrument, which includes Coastal Blue, Blue, Green I, Green, Yellow, Red, Red Edge, and NIR, beginning in 2020. Surface Reflectance (SR) products were selected to ensure consistency across varying atmospheric conditions, thereby minimizing uncertainty in the spectral response across time and location. Thus, these multispectral imagery products are specially designed for temporal analysis and monitoring applications. SR is derived from the standard Analytic Product (radiance), which is processed to top-of-atmosphere reflectance and then atmospherically corrected to bottom-of-atmosphere reflectance.

We acquired 33 satellite images covering 1233 km^2 of Mediterranean coastal areas and islands for 2023 (see Supporting Information, Table S1). Images were acquired over several days under clear-sky conditions between June and September, when seagrass and algal biomass were abundant. The chosen sites were selected to minimize evident local human disturbance, thereby reducing the potential confounding influence of direct anthropogenic impacts on fragmentation patterns.

4.6 | Data Pre-Processing

The NIR band, which is strongly attenuated by water, was used to mask land pixels using a simple clustering algorithm (K-means) and was subsequently replaced with bathymetry data. We then masked all pixels with depths greater than 30 m, as the AI model's performance is significantly reduced beyond this threshold (Giménez-Romero et al. 2025). The resulting processed satellite images were used as input data to obtain habitat estimates.

4.7 | Habitat Estimates

We employed the deep learning framework developed by Giménez-Romero et al. (2025) to estimate the spatial cover of different benthic habitats, including *Posidonia oceanica*, across 33 selected coastal locations in the Mediterranean Sea. The framework, based on convolutional neural networks (CNNs), classifies each pixel of the pre-processed satellite imagery into one of four ecologically meaningful benthic classes: (1) rocks and brown algae, (2) sandy bottoms, (3) *Posidonia oceanica*, and (4) other green plants (e.g., *Cymodocea nodosa*). The model was trained on an extensive, georeferenced dataset of benthic habitat maps spanning diverse environmental conditions across the Balearic Sea, achieving robust generalization with a mean Intersection over Union (IoU) of 77.30% for the *P. oceanica* class in independent cross-regional validation and a median IoU of 95.22% in the final consensus model trained on the full dataset (Giménez-Romero et al. 2025).

We applied the final, fully trained model to the 33 Planet surface reflectance images. Each image was processed at a native 3–4 m resolution, yielding high-fidelity habitat maps that resolve fine-scale meadow boundaries, internal patch structures, and fragmentation patterns (see Figures S1–S3 for some examples). The resulting habitat maps, covering a cumulative coastal area of 1233 km^2, served as the base dataset for all subsequent analyzes.

4.8 | Estimation of *Posidonia oceanica* Cover

The cover of *Posidonia oceanica* in each satellite image was computed as follows:

$$C = \frac{A_{Posidonia}}{A_{tot}}, \tag{7}$$

where A_P represents the area of *Posidonia oceanica*, and A_{tot} is the total area of the studied zone, that is, the area of the satellite image that is classified as any of the benthic categories.

4.9 | Fragmentation Analysis

To quantify the spatial fragmentation of *Posidonia oceanica* meadows, we computed two complementary fragmentation indices designed to capture distinct ecological aspects of the seagrass spatial structure.

We first calculated a gap-weighted fragmentation index (FI) adapted from the urban fragmentation metric (De Montis et al. 2020, 2021) and applied it to seagrass systems to assess the ecological impact of discontinuities on productivity (Swadling et al. 2023). This index accounts for both the area of bare sand within a defined landscape unit and the spatial configuration of gaps within the seagrass matrix.

$$\mathrm{FI} = (1 - C)\frac{P_{cont}}{\sqrt{\pi(A_{\mathrm{tot}} - A_{veg})}} \tag{8}$$

Here, A_{tot} is the total area considered, A_{veg} is the vegetated area, and P_{cont} represents the contact perimeter between the vegetated and unvegetated areas. The first term captures the proportion of the landscape that is unvegetated, whereas the second term describes the geometric complexity of the gaps, weighted by their perimeter-to-area relationship. This index ranges from 0 (fully continuous meadow) to 1 (highly fragmented meadow) and is

sensitive to both the abundance and spatial configuration of non-vegetated patches embedded within the meadow.

To complement this measure, we computed a composite fragmentation index based on a suite of landscape-level metrics widely used in landscape and seascape ecology (Sleeman et al. 2005; McGarigal et al. 2005; Santos et al. 2016). These metrics were calculated from binary habitat maps using the `landscapemetrics` package in R (Hesselbarth et al. 2019) and included the following:

- Patch density (PD)—number of discrete seagrass patches per unit area, reflecting the degree of habitat subdivision.
- Landscape division index (LD)—the probability that two randomly chosen locations in the landscape belong to different patches, increasing with fragmentation.
- Area-weighted mean perimeter-to-area ratio (AWMPAR) – a measure of patch compactness and edge complexity.
- Mean radius of gyration (GYRATE) – describes the average distance between cells within a patch, serving as a proxy for patch cohesion.
- Number of holes – quantifies internal perforations within seagrass patches and is calculated using the 'Union' tool in ArcGIS. This value was normalized per hectare of seagrass to account for variations in overall coverage.

All metrics were standardized (min-max normalization) and integrated into a single composite fragmentation index (Santos et al. 2016, 2022). Following this previous composite fragmentation indicator, standardized metrics were combined using equal weights because no independent empirical basis was available to assign differential weights to the individual landscape metrics. Sensitivity to alternative weighting schemes therefore remains a methodological uncertainty of the composite index. The resulting index ranged from 0 (low fragmentation) to 1 (high fragmentation), providing a unified metric for cross-site comparisons.

Together, these two approaches provide complementary perspectives on seagrass fragmentation: one emphasizes the influence of internal bare-sand gaps, whereas the other captures broader changes in patch configuration. We used both indices to assess the relationship between fragmentation and thermal stress across the study sites.

To assess whether the fragmentation patterns were robust to index choice, we compared the two indices in two complementary ways (Supporting Information Section 5). First, we related each index to the number of isolated *P. oceanica* patches, a direct and interpretable proxy for spatial fragmentation (Figure S9). Second, we compared the site rankings obtained from each index to test whether both metrics produced a consistent ordering of sites along the fragmentation gradient (Figure S11). Both analyzes revealed a strong correlation between the two indices and a consistent ranking of sites, supporting the robustness of our fragmentation assessments.

4.10 | Data and Code Availability

The CAMELE deep learning model used to estimate *Posidonia oceanica* cover is openly available at (Giménez-Romero 2024). Because satellite imagery was obtained from Planet under the Education and Research Program, which provides limited non-commercial access to PlanetScope and RapidEye imagery, we cannot share the raw images. However, all scripts and workflows used to compute Stress Degree Days (SDD), thermal stress, fragmentation indices, and seagrass cover are publicly available in a GitHub repository (Giménez-Romero 2025a) and archived in Zenodo (Giménez-Romero 2025b). All datasets generated in this study, including the predicted *P. oceanica* habitat maps for the selected regions, SDD and thermal stress values for the Mediterranean Sea (historical period 2000–2020), and projected values under RCP4.5 and RCP8.5 scenarios (2006–2100), are available through the Zenodo repository.

Author Contributions

Tomàs Sintes: conceptualization, investigation, funding acquisition, writing – review and editing, supervision. **Àlex Giménez-Romero:** conceptualization, investigation, writing – original draft, methodology, validation, visualization, writing – review and editing, formal analysis, software, data curation. **Manuel A. Matías:** conceptualization, investigation, writing – review and editing, supervision. **Carlos M. Duarte:** investigation, writing – review and editing, supervision.

Acknowledgements

We acknowledge Nuria Marbà, Elvira Mayol, and Damià Gomila for their valuable comments and suggestions. We also acknowledge Planet Labs for access to satellite imagery data under their Education and Research Program. This work was supported by grants TED2021-131836B-I00 (SEDIMENT) funded by the Spanish Ministry of Science and Innovation MICIU/AEI/https://doi.org/10.13039/501100011033 and by the European Union NextGenerationEU/PRTR Program; PID2021-123723OB-C22 (CYCLE) and PID2024-156062OB-I00 (CHANGE-ME) funded by MICIU/AEI/https://doi.org/10.13039/501100011033 and by ERDF, EU; and CEX2021-001164-M (María de Maeztu Program for Units of Excellence in R&D) funded by MICIU/AEI/https://doi.org/10.13039/501100011033. À.G. R. acknowledges financial support from grant JDC2024-053275-I, funded by MICIU/AEI/https://doi.org/10.13039/501100011033 and FSE+; and from grant PID2021-124731NB-I00, funded by the Spanish Ministry of Science and Innovation MICIU/AEI/https://doi.org/10.13039/501100011033 and by ERDF, EU. C.M.D. was supported by King Abdullah University of Science and Technology through baseline funding.

Funding

This work was supported by Ministerio de Ciencia, Innovación y Universidades (Grants TED2021-131836B-I00, PID2021-123723OB-C22, CEX2021-001164-M, and JDC2024-053275-I).

Conflicts of Interest

The authors declare no conflicts of interest.

Data Availability Statement

The data that support the findings of this study are openly available in Zenodo at https://zenodo.org/records/17476416, reference number https://doi.org/10.5281/zenodo.17476416.

References

Bakirman, T., and M. U. Gumusay. 2020. "Assessment of Machine Learning Methods for Seagrass Classification in the Mediterranean." *Baltic Journal of Modern Computing* 8: 315–326.

Barbier, E. B., S. D. Hacker, C. Kennedy, E. W. Koch, A. C. Stier, and B. R. Silliman. 2011. "The Value of Estuarine and Coastal Ecosystem Services." *Ecological Monographs* 81: 169–193.

Bennett, S., T. Alcoverro, D. Kletou, et al. 2024. "Warm and Cool-Edge Populations Reveal High Resilience of Seagrass (*Posidonia oceanica*) to Warming." *Authorea*. https://doi.org/10.22541/au.170666863.36526783/v1.

Bennett, S., G. Roca, R. Vaquer-Sunyer, et al. 2022. "Thermal Performance of Seaweeds and Seagrasses Across a Regional Climate Gradient." *Frontiers in Marine Science* 9: 733315.

Borum, J., O. Pedersen, T. M. Greve, et al. 2005. "The Potential Role of Plant Oxygen and Sulphide Dynamics in Die-Off Events of the Tropical Seagrass, *Thalassia testudinum*." *Journal of Ecology* 93: 148–158.

Bos, A. R., T. J. Bouma, G. L. de Kort, and M. M. van Katwijk. 2007. "Ecosystem Engineering by Annual Intertidal Seagrass Beds: Sediment Accretion and Modification." *Estuarine, Coastal and Shelf Science* 74: 344–348.

Catucci, E., and M. Scardi. 2020. "A Machine Learning Approach to the Assessment of the Vulnerability of *Posidonia oceanica* Meadows." *Ecological Indicators* 108: 105744.

Chand, S., and B. Bollard. 2022. "Detecting the Spatial Variability of Seagrass Meadows and Their Consequences on Associated Macrofauna Benthic Activity Using Novel Drone Technology." *Remote Sensing* 14: 160.

Chefaoui, R. M., C. M. Duarte, and E. A. Serrão. 2018. "Dramatic Loss of Seagrass Habitat Under Projected Climate Change in the Mediterranean Sea." *Global Change Biology* 24: 4919–4928.

Chimienti, G., A. Tursi, M. Maiorca, and F. Mastrototaro. 2025. "Flowering of *Posidonia oceanica* in the Italian Adriatic Sea Following the 2024 Marine Heatwave." *Estuarine, Coastal and Shelf Science* 324: 109483.

Chowdhury, M., A. Martínez-Sansigre, M. Mole, et al. 2024. "AI-Driven Remote Sensing Enhances Mediterranean Seagrass Monitoring and Conservation to Combat Climate Change and Anthropogenic Impacts." *Scientific Reports* 14: 8360.

Copernicus Climate Change Service. 2020. "Marine Biogeochemistry Data for the Northwest European Shelf and Mediterranean Sea From 2006 up to 2100 Derived From Climate Projections." https://doi.org/10.24381/cds.dcc9295c.

Copernicus Climate Change Service (C3S). 2019. *Sea Surface Temperature Daily Data From 1981 to Present Derived From Satellite Observations*. https://doi.org/10.24381/cds.cf608234.

Dai, J., K. He, and J. Sun. 2016. "Instance-Aware Semantic Segmentation via Multi-Task Network Cascades." In *Proceedings of the IEEE Conference on Computer Vision and Pattern Recognition*, 3150–3158. IEEE.

De Montis, A., V. Serra, G. Calia, D. Trogu, and A. Ledda. 2021. "To Weight or Not to Weight, That Is the Question: The Design of a Composite Indicator of Landscape Fragmentation." *Applied Sciences* 11: 3208.

De Montis, A., V. Serra, A. Ganciu, and A. Ledda. 2020. "Assessing Landscape Fragmentation: A Composite Indicator." *Sustainability* 12: 9632.

Duarte, C., E. T. Apostolaki, O. Serrano, A. Steckbauer, and R. K. F. Unsworth. 2025. "Conserving Seagrass Ecosystems to Meet Global Biodiversity and Climate Goals." *Nature Reviews Biodiversity* 1: 150–165.

Duarte, C. M., and C. L. Chiscano. 1999. "Seagrass Biomass and Production: A Reassessment." *Aquatic Botany* 65: 159–174.

Duarte, C. M., I. J. Losada, I. E. Hendriks, I. Mazarrasa, and N. Marbà. 2013. "The Role of Coastal Plant Communities for Climate Change Mitigation and Adaptation." *Nature Climate Change* 3: 961–968.

Duarte, C. M., T. Sintes, and N. Marbà. 2013. "Assessing the CO_2 Capture Potential of Seagrass Restoration Projects." *Journal of Applied Ecology* 50: 1341–1349.

Gacia, E., and C. Duarte. 2001. "Sediment Retention by a Mediterranean *Posidonia oceanica* Meadow: The Balance Between Deposition and Resuspension." *Estuarine, Coastal and Shelf Science* 52: 505–514.

Giménez-Romero, À. 2024. *CAMELE: Consensus for Automated Marine Ecosystem Labelling and Evaluation*. Zenodo. https://doi.org/10.5281/zenodo.10792281.

Giménez-Romero, À. 2025a. https://github.com/agimenezromero/Thermal-stress-drives-seagrass-fragmentation-in-the-Mediterranean-Sea.

Giménez-Romero, À. 2025b. "Thermal Stress Drives Seagrass Fragmentation in the Mediterranean Sea." https://doi.org/10.5281/zenodo.17476416.

Giménez-Romero, À., D. Ferchichi, P. Moreno-Spiegelberg, T. Sintes, and M. A. Matías. 2025. "A Generalizable Deep Learning Framework for Large-Scale Mapping of Seagrass Habitats." *Ecological Indicators* 180: 114349.

Granata, T., T. Serra, J. Colomer, X. Casamitjana, C. Duarte, and E. Gacia. 2001. "Flow and Particle Distributions in a Nearshore Seagrass Meadow Before and After a Storm." *Marine Ecology Progress Series* 218: 95–106.

Harald, H.-S. 2023. "Detrimental Impact of Sulfide on the Seagrass *Zostera marina* in Dark Hypoxia." *PLoS One* 18: e0295450.

Helber, S. B., G. Procaccini, E. F. Belshe, et al. 2021. "Unusually Warm Summer Temperatures Exacerbate Population and Plant Level Response of *Posidonia oceanica* to Anthropogenic Nutrient Stress." *Frontiers in Plant Science* 12: 662682.

Hendriks, I. E., T. Sintes, T. J. Bouma, and C. M. Duarte. 2008. "Experimental Assessment and Modeling Evaluation of the Effects of the Seagrass *Posidonia oceanica* on Flow and Particle Trapping." *Marine Ecology Progress Series* 356: 163–173.

Hesselbarth, M. H. K., M. Sciaini, K. A. With, K. Wiegand, and J. Nowosad. 2019. "Landscapemetrics: An Open-Source R Tool to Calculate Landscape Metrics." *Ecography* 42: 1648–1657.

Jahnke, M., D. D'Esposito, L. Orrù, et al. 2019. "Adaptive Responses Along a Depth and a Latitudinal Gradient in the Endemic Seagrass *Posidonia oceanica*." *Heredity* 122: 233–243.

Jeon, E., S. Kim, S. Park, J. Kwak, and I. Choi. 2021. "Semantic Segmentation of Seagrass Habitat From Drone Imagery Based on Deep Learning: A Comparative Study." *Ecological Informatics* 66: 101430.

Jorda, G., N. Marbà, S. Bennett, J. Santana-Garcon, S. Agusti, and C. M. Duarte. 2020. "Ocean Warming Compresses the Three-Dimensional Habitat of Marine Life." *Nature Ecology & Evolution* 4: 109–114.

Jordà, G., N. Marbà, and C. M. Duarte. 2012. "Mediterranean Seagrass Vulnerable to Regional Climate Warming." *Nature Climate Change* 2: 821–824.

Kellaris, A., A. Gil, J. Faria, et al. 2019. "Using Low-Cost Drones to Monitor Heterogeneous Submerged Seaweed Habitats: A Case Study in the Azores." *Aquatic Conservation: Marine and Freshwater Ecosystems* 29: 1909–1922.

Kendrick, G. A., R. J. Orth, J. Statton, et al. 2017. "Demographic and Genetic Connectivity: The Role and Consequences of Reproduction, Dispersal and Recruitment in Seagrasses." *Biological Reviews* 92: 921–938.

Klein, S. G., C. Roch, and C. M. Duarte. 2024. "Systematic Review of the Uncertainty of Coral Reef Futures Under Climate Change." *Nature Communications* 15: 2224.

Koch, E. W., J. D. Ackerman, J. Verduin, and M. v. Keulen. 2006. "Fluid Dynamics in Seagrass Ecology—From Molecules to Ecosystems."

In *Seagrasses: Biology, Ecology, and Conservation*, 193–225. Springer-Verlag.

Litsi-Mizan, V., P. T. Efthymiadis, V. Gerakaris, O. Serrano, M. Tsapakis, and E. T. Apostolaki. 2023. "Decline of Seagrass (*Posidonia oceanica*) Production Over Two Decades in the Face of Warming of the Eastern Mediterranean Sea." *New Phytologist* 239: 2126–2137.

Madsen, J. D., P. A. Chambers, W. F. James, E. W. Koch, and D. F. Westlake. 2001. "The Interaction Between Water Movement, Sediment Dynamics and Submersed Macrophytes." *Hydrobiologia* 444: 71–84.

Marbà, N., E. Díaz-Almela, and C. M. Duarte. 2013. *Posidonia oceanica Changes in the Mediterranean Sea*. Digital.CSIC. https://digital.csic.es/handle/10261/88165.

Marbà, N., E. Díaz-Almela, and C. M. Duarte. 2014. "Mediterranean Seagrass (*Posidonia oceanica*) Loss Between 1842 and 2009." *Biological Conservation* 176: 183–190.

Marbà, N., and C. M. Duarte. 2010. "Mediterranean Warming Triggers Seagrass (*Posidonia oceanica*) Shoot Mortality." *Global Change Biology* 16: 2366–2375.

Marbà, N., G. Jorda, S. Agusti, C. Girard, and C. M. Duarte. 2015. "Footprints of Climate Change on Mediterranean Sea Biota." *Frontiers in Marine Science* 2: 56.

Marbà, N., G. Jordà, S. Bennett, and C. M. Duarte. 2022. "Seagrass Thermal Limits and Vulnerability to Future Warming." *Frontiers in Marine Science* 9: 868026.

Marín-Guirao, L., L. Entrambasaguas, J. M. Ruiz, and G. Procaccini. 2019. "Heat-Stress Induced Flowering Can Be a Potential Adaptive Response to Ocean Warming for the Iconic Seagrass *Posidonia oceanica*." *Molecular Ecology* 28: 2486–2501.

Martín Míguez, B., A. Novellino, M. Vinci, et al. 2019. "The European Marine Observation and Data Network (EMODnet): Visions and Roles of the Gateway to Marine Data in Europe." *Frontiers in Marine Science* 6: 313.

Mayol, E., P. A. Aramburu, C. A. M. Lujan-Williams, et al. 2026. "Effects of Moderate Meadow Fragmentation and Hydrodynamics on the Water Column Oxygenation by the Seagrass *Posidonia oceanica*." *Submitted for publication*.

McGarigal, K., S. Cushman, and C. Regan. 2005. *Quantifying Terrestrial Habitat Loss and Fragmentation: A Protocol*, 113. University of Massachusetts, Department of Natural Resources Conservation.

Mcleod, E., G. L. Chmura, S. Bouillon, et al. 2011. "A Blueprint for Blue Carbon: Toward an Improved Understanding of the Role of Vegetated Coastal Habitats in Sequestering CO2." *Frontiers in Ecology and the Environment* 9: 552–560.

Millennium Ecosystem Assessment. 2005. *Ecosystems and Human Well-Being: A Framework Working Group for Assessment Report of the Millennium Ecosystem Assessment*. Island Press. https://www.millenniumassessment.org/documents/document.356.aspx.pdf.

Ondiviela, B., I. J. Losada, J. L. Lara, et al. 2014. "The Role of Seagrasses in Coastal Protection in a Changing Climate." *Coastal Engineering* 87: 158–168.

Ontoria, Y., A. Cuesta-Gracia, J. M. Ruiz, J. Romero, and M. Pérez. 2019. "The Negative Effects of Short-Term Extreme Thermal Events on the Seagrass *Posidonia oceanica* Are Exacerbated by Ammonium Additions." *PLoS One* 14: e0222798.

Pansini, A., M. Bosch-Belmar, M. Berlino, G. Sarà, and G. Ceccherelli. 2022. "Collating Evidence on the Restoration Efforts of the Seagrass *Posidonia oceanica*: Current Knowledge and Gaps." *Science of the Total Environment* 851: 158320.

Pazzaglia, J., L. Marín-Guirao, L. Ambrosino, et al. 2025. "Handling the Heat: Ocean Acidification Mitigates the Effects of Marine Heatwaves on *Posidonia oceanica* Seedlings." *Journal of Experimental Botany* 76: eraf276.

Planet Team. 2017. "Planet Application Program Interface: In Space for Life on Earth." https://api.planet.com.

Poursanidis, D., K. Topouzelis, and N. Chrysoulakis. 2018. "Mapping Coastal Marine Habitats and Delineating the Deep Limits of the Neptune's Seagrass Meadows Using Very High Resolution Earth Observation Data." *International Journal of Remote Sensing* 39: 8670–8687.

Power, S., F. Delage, G. Wang, I. Smith, and G. Kociuba. 2017. "Apparent Limitations in the Ability of CMIP5 Climate Models to Simulate Recent Multi-Decadal Change in Surface Temperature: Implications for Global Temperature Projections." *Climate Dynamics* 49: 53–69.

Rahman, M. A., and Y. Wang. 2016. "Optimizing Intersection-Over-Union in Deep Neural Networks for Image Segmentation." In *Advances in Visual Computing*, edited by G. Bebis, 234–244. Springer International Publishing.

Ravaglioli, C., L. de Marchi, S. Anselmi, et al. 2024. "Ocean Acidification Impairs Seagrass Performance Under Thermal Stress in Shallow and Deep Water." *Environmental Research* 241: 117629.

Rigo, I., C. Paoli, G. Dapueto, et al. 2021. "The Natural Capital Value of the Seagrass *Posidonia oceanica* in the North-Western Mediterranean." *Diversity* 13: 499.

Rinaldi, A., M. Martinez, F. Badalamenti, et al. 2023. "The Ontogeny-Specific Thermal Sensitivity of the Seagrass *Posidonia oceanica*." *Frontiers in Marine Science* 10: 1183728.

Romanski, J., A. Romanou, M. Bauer, and G. Tselioudis. 2014. "Teleconnections, Midlatitude Cyclones and Aegean Sea Turbulent Heat Flux Variability on Daily Through Decadal Time Scales." *Regional Environmental Change* 14: 1713–1723.

Ruiz-Reynés, D., D. Gomila, T. Sintes, E. Hernández-García, N. Marbà, and C. M. Duarte. 2017. "Fairy Circle Landscapes Under the Sea." *Science Advances* 3: e1603262.

Ruiz-Reynés, D., E. Mayol, T. Sintes, et al. 2023. "Self-Organized Sulfide-Driven Traveling Pulses Shape Seagrass Meadows." *Proceedings of the National Academy of Sciences* 120: e2216024120.

Sánchez-Garrido, J. C., and I. Nadal. 2022. "The Alboran Sea Circulation and Its Biological Response: A Review." *Frontiers in Marine Science* 9: 933390.

Santana-Garcon, J., S. Bennett, N. Marbà, A. Vergés, R. Arthur, and T. Alcoverro. 2023. "Tropicalization Shifts Herbivore Pressure From Seagrass to Rocky Reef Communities." *Proceedings of the Royal Society B: Biological Sciences* 290: 20221744.

Santos, R. O., W. R. James, J. A. Nelson, et al. 2022. "Influence of Seascape Spatial Pattern on the Trophic Niche of an Omnivorous Fish." *Ecosphere* 13: e3944.

Santos, R. O., D. Lirman, and S. J. Pittman. 2016. "Long-Term Spatial Dynamics in Vegetated Seascapes: Fragmentation and Habitat Loss in a Human-Impacted Subtropical Lagoon." *Marine Ecology* 37: 200–214.

Savva, I., S. Bennett, G. Roca, G. Jordà, and N. Marbà. 2018. "Thermal Tolerance of Mediterranean Marine Macrophytes: Vulnerability to Global Warming." *Ecology and Evolution* 8: 12032–12043.

Schott, F., M. Visbeck, U. Send, J. Fischer, L. Stramma, and Y. Desaubies. 1996. "Observations of Deep Convection in the Gulf of Lions, Northern Mediterranean, During the Winter of 1991/92." *Journal of Physical Oceanography* 26: 505–524.

Sleeman, J. C., G. A. Kendrick, G. S. Boggs, and B. J. Hegge. 2005. "Measuring Fragmentation of Seagrass Landscapes: Which Indices Are Most Appropriate for Detecting Change?" *Marine and Freshwater Research* 56: 851–864.

Stipcich, P., G. Ceccherelli, L. Marín-Guirao, J. Pazzaglia, A. Santillán-Sarmiento, and G. Procaccini. 2024. "The Intensity of a Field Simulated

Marine Heat Wave Differentially Modulates the Transcriptome Expression of *Posidonia oceanica* From Warm and Cold Environments." *Marine Biology* 171: 192.

Stipcich, P., V. Resaikos, and G. Ceccherelli. 2023. "Experimental Thermocline Deepening Highlights the Resilience of the Seagrass *Posidonia oceanica*: An Opportunity to Investigate Shoot Adaptability." *Marine Pollution Bulletin* 189: 114824.

Swadling, D. S., G. J. West, P. T. Gibson, R. J. Laird, and T. M. Glasby. 2023. "Don't Go Breaking Apart: Anthropogenic Disturbances Predict Meadow Fragmentation of an Endangered Seagrass." *Aquatic Conservation: Marine and Freshwater Ecosystems* 33: 56–69.

Telesca, L., A. Belluscio, A. Criscoli, et al. 2015. "Seagrass Meadows (*Posidonia oceanica*) Distribution and Trajectories of Change." *Scientific Reports* 5: 12505.

Traganos, D., B. Aggarwal, D. Poursanidis, K. Topouzelis, N. Chrysoulakis, and P. Reinartz. 2018. "Towards Global-Scale Seagrass Mapping and Monitoring Using Sentinel-2 on Google Earth Engine: The Case Study of the Aegean and Ionian Seas." *Remote Sensing* 10: 1–14.

Traganos, D., and P. Reinartz. 2018. "Mapping Mediterranean Seagrasses With Sentinel-2 Imagery." *Marine Pollution Bulletin* 134: 197–209.

van de Vijsel, R. C., E. Hernández-García, A. Orfila, and D. Gomila. 2023. "Optimal Wave Reflection as a Mechanism for Seagrass Self-Organization." *Scientific Reports* 13: 20278.

Waycott, M., C. M. Duarte, T. J. B. Carruthers, et al. 2009. "Accelerating Loss of Seagrasses Across the Globe Threatens Coastal Ecosystems." *Proceedings of the National Academy of Sciences* 106: 12377–12381.

Supporting Information

Additional supporting information can be found online in the Supporting Information section. **Table S1:** Satellite images used for habitat classification. A summary of the PlanetScope satellite imagery dataset used to estimate *Posidonia oceanica* cover across the Mediterranean Sea. The table reports the geographic coordinates (to the 4th decimal) and acquisition dates for each site. All images correspond to the summer months (June–September), when seagrass biomass is highest. **Figure S1:** Example of deep learning-based benthic habitat classification for *Posidonia oceanica*. (a) True-color composite of high-resolution PlanetScope satellite imagery (3–4 m resolution) for the coast of Alexandria. (b) Corresponding CNN model prediction showing classified habitats: *P. oceanica* (green), bare sediment (yellow), macroalgae/rock (brown), and other green plants (cyan). **Figure S2:** (a) True-color composite of high-resolution PlanetScope satellite imagery (3–4 m resolution) for the coast of Sicily. (b) Corresponding CNN model prediction showing classified habitats: *P. oceanica* (green), bare sediment (yellow), macroalgae/rock (brown), and other green plants (cyan). **Figure S3:** (a) True-color composite of high-resolution PlanetScope satellite imagery (3–4 m resolution) for the coast of Sardinia. (b) Corresponding CNN model prediction showing classified habitats: *P. oceanica* (green), bare sediment (yellow), macroalgae/rock (brown), and other green plants (cyan). **Figure S4:** Logistic fit relating SDD to observed shoot mortality under constant temperature conditions derived from the experiments from Savva et al. (2018). **Figure S5:** Spatial distribution of independent field observations used to evaluate the consistency of the Stress Degree Days (SDD) framework with reported *Posidonia oceanica* decline across the Mediterranean Sea. Points indicate the locations of field-derived observations of meadow deterioration compiled from independent studies. Colors indicate the estimated thermal stress at each location, computed from the SDD framework using historical sea surface temperature records. This dataset provides an external field-based comparison for the thermal exposure metric, although its spatial coverage, sampling design, and response variables are heterogeneous. **Figure S6:** Relationship between Stress Degree Days (SDD) and independent field-derived indicators of *Posidonia oceanica* deterioration across the Mediterranean Sea. Each panel shows the association between site-level SDD and a different field response variable: shoot density change, percent area lost, percent area degraded, percent area affected, absolute extent change, and cover change. Correlation coefficients and associated *p*-values are shown within each panel. Overall, field indicators of meadow deterioration tend to vary in the expected direction with increasing cumulative thermal exposure, with the clearest relationship observed for shoot density change. Because the compiled field datasets differ in sampling design, temporal window, response variable, and local environmental context, these comparisons should be interpreted as an external consistency check rather than as a causal validation of the SDD–mortality relationship under natural field conditions. **Figure S7:** Relationship between SDD-derived thermal stress and independent field-derived indicators of *Posidonia oceanica* deterioration across the Mediterranean Sea. Thermal stress was obtained by transforming accumulated SDD values through the logistic mortality function parameterized from experimental thermal-response data. Each panel shows the association between estimated thermal stress and a different field response variable: shoot density change, percent area lost, percent area degraded, percent area affected, absolute extent change, and cover change. Correlation coefficients and associated *p*-values are shown within each panel. The results are broadly consistent with those obtained using raw SDD values, supporting the interpretation of the SDD framework as a physiologically informed exposure metric. However, these relationships remain observational and should not be interpreted as definitive field validation of the laboratory-derived mortality function. **Figure S8:** Relationship between the maximum temperature and seagrass condition. (a) Relationship between maximum monthly sea surface temperature (T_{max}) and *P. oceanica* cover across Mediterranean sites. (b) Relationship between T_{max} and the fragmentation index. The dashed orange line indicates the lethal temperature threshold (LT_{50} = 28.9°C) as reported by Savva et al. (2018). Both panels show that while mortality-based thresholds capture the upper limit of thermal stress, substantial degradation in meadow condition occurs well below LT_{50}. **Figure S9:** Comparison between the two fragmentation indices. Correlation between the gap-weighted fragmentation index (FI, following Mayol et al. 2026) and the composite landscape fragmentation index (Swadling et al. 2023). Both indices exhibited strong positive correlations with the number of meadow patches, indicating consistent sensitivity to structural discontinuities. Regression statistics (R^2 and *p* values) are shown for each relationship. **Figure S10:** Relationship between thermal stress and fragmentation. Scatterplot showing the relationship between cumulative thermal stress (SDD) and composite fragmentation index. Fragmentation increases with thermal stress, consistent with an association between cumulative sublethal warming and meadow spatial disaggregation. **Figure S11:** Rank consistency between the two fragmentation indices. Each point represents one study site, ranked independently according to the gap-weighted fragmentation index and the composite landscape fragmentation index. The dashed line indicates the 1:1 relationship expected if both indices produced identical site rankings. The strong positive association indicates that the two indices provide broadly consistent ordering of sites along the fragmentation gradient, while deviations from the 1:1 line reflect their sensitivity to complementary aspects of meadow spatial structure. **Figure S12:** Patch size and inter-patch distance distributions. (a) Probability density function of patch size across all study sites, showing a broad, heavy-tailed distribution characteristic of spatial fragmentation processes. The slope of the fitted power-law ($\beta = 1.56$) reflects scale-invariant structure in meadow patchiness. (b) Distribution of inter-patch distances, which also follows an approximate power-law ($\beta = 2.38$), consistent with self-organized spatial clustering in *P. oceanica* meadows. **Figure S13:** Projected thermal stress under climate change scenarios. Spatial distribution of cumulative thermal stress (SDD) in the Mediterranean Sea under future climate projections. Maps correspond to RCP4.5 and RCP8.5 scenarios based on simulations from the Copernicus "Marine Biogeochemistry Data for the Northwest European Shelf and Mediterranean Sea" dataset (Copernicus Climate Change Service 2020). The depicted projections correspond to the average results from the indicated time periods. The results highlight a northward expansion of high-stress areas, indicating potential large-scale degradation of *P. oceanica* meadows under continued warming. **Figure S14:** Projected seagrass cover under climate change scenarios. Projected *Posidonia oceanica* cover under RCP4.5 (left column) and RCP8.5 (right column) scenarios for 2006, 2050, 2080, and 2099 (rows from top to bottom). Maps show the projected cover derived from the correlation between current SDD and observed seagrass cover across the

Mediterranean. **Figure S15:** Projected seagrass cover change under climate change scenarios. Projected *Posidonia oceanica* cover change under RCP4.5 (left column) and RCP8.5 (right column) scenarios for 2006, 2050, 2080, and 2099 (rows from top to bottom). Maps show the projected change in cover derived from the correlation between current SDD and observed seagrass cover across the Mediterranean. **Figure S16:** Projected seagrass fragmentation under climate change scenarios. Projected *Posidonia oceanica* fragmentation under RCP4.5 (left column) and RCP8.5 (right column) scenarios for 2006, 2050, 2080, and 2099 (rows from top to bottom). Maps show the projected fragmentation derived from the correlation between current SDD and observed seagrass fragmentation across the Mediterranean. **Figure S17:** Projected thermal stress across depths under the RCP8.5 scenario. (a) Spatial distribution of cumulative thermal stress (SDD) at 10 m depth in 2100 under the RCP8.5 scenario. The redder areas indicate higher thermal stress, ranging from 0 (no stress) to 1 (maximum stress). (b) Spatial distribution of cumulative thermal stress (SDD) at 20 m depth in 2100 under the RCP8.5 scenario, showing a reduced intensity compared to 10 m. (c) Average percentage of high-stress areas (> 50%) across the Mediterranean Sea as a function of depth for different time periods (2006–2016, 2020–2030, 2040–2050, 2080–2090, and 2090–2100). The plot illustrates a projected increase in high-stress areas over time, with a sharp decline in their extent beyond 20–30 m depth, highlighting the shallow-water vulnerability.